ACS APPLIED MATERIALS & INTERFACES

Research Article

www.acsami.org

In Situ Generation of Cellulose Nanocrystals in Polycaprolactone Nanofibers: Effects on Crystallinity, Mechanical Strength, Biocompatibility, and Biomimetic Mineralization

Mahesh Kumar Joshi,[†,‡] Arjun Prasad Tiwari,[†] Hem Raj Pant,[§] Bishnu Kumar Shrestha,[†] Han Joo Kim,[†,∥] Chan Hee Park,[*,†] and Cheol Sang Kim[*,†,⊥,#]

[†]Department of Bionanosystem Engineering, Graduate School, Chonbuk National University, Jeonju 561-756, Republic of Korea

[‡]Department of Chemistry, Tri-Chandra Multiple Campus, and [§]Department of Engineering Science and Humanities, Institute of Engineering, Pulchowk Campus, Tribhuvan University, Kathmandu, Nepal

[∥]Department of Convergence Technology Engineering, College of engineering, Chonbuk National University, Jeonju 561-756, Republic of Korea

[⊥]Division of Mechanical Design Engineering, Chonbuk National University, Jeonju 561-756, Republic of Korea

[#]Eco-friendly machine parts design research center, Chonbuk National University, Jeonju 561-756, Republic of Korea

Supporting Information

ABSTRACT: Post-electrospinning treatment is a facile process to improve the properties of electrospun nanofibers for various applications. This technique is commonly used when direct electrospinning is not a suitable option to fabricate a nonwoven membrane of the desired polymer in a preferred morphology. In this study, a representative natural-synthetic hybrid of cellulose acetate (CA) and polycaprolactone (PCL) in different ratios was fabricated using an electrospinning process, and CA in the hybrid fiber was transformed into cellulose (CL) by post-electrospinning treatment via alkaline saponification. Scanning electron microscopy was employed to study the effects of polymer composition and subsequent saponification on the morphology of the nanofibers. Increasing the PCL content in the PCL/CA blend solution caused a gradual decrease in viscosity, resulting in smoother and more uniform fibers. The saponification of fibers lead to pronounced changes in the physicochemical properties. The crystallinity of the PCL in the composite fiber was varied according to the composition of the component polymers. The water contact angle was considerably decreased (from 124° to less than 20°), and the mechanical properties were greatly enhanced (Young's Modulus was improved by ≈20−30 fold, tensile strength by 3−4 fold, and tensile stress by ≈2−4 fold) compared to those of PCL and PCL/CA membranes. Regeneration of cellulose chains in the nanofibers increased the number of hydroxyl groups, which increased the hydrogen bonding, thereby improving the mechanical properties and wettability of the composite nanofibers. The improved wettability and presence of surface functional groups enhanced the ability to nucleate bioactive calcium phosphate crystals throughout the matrix when exposed to a simulated body fluid solution. Experimental results of cell viability assay, confocal microscopy, and scanning electron microscopy imaging showed that the fabricated nanofibrous membranes have excellent ability for MC3T3-E1 cell proliferation and growth. Given the versatility and widespread use of cellulose−synthetic hybrid systems in the construction of tissue-engineered scaffolds, this work provides a novel strategy to fabricate the biopolymer-based materials for applications in tissue engineering and regenerative medicine.

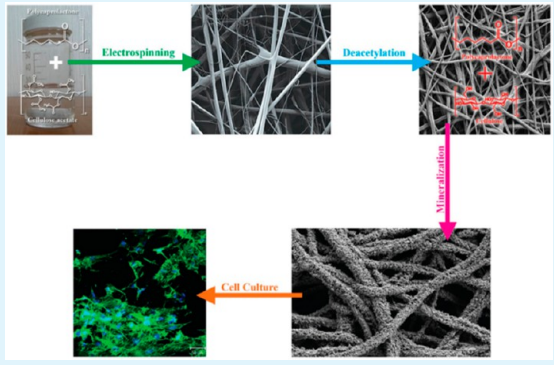

KEYWORDS: *electrospinning, composite fiber, post-electrospinning treatment, alkaline saponification, cellulose nanocrystals, biomimetic mineralization*

1. INTRODUCTION

The development of micro-/nanofibers has attracted significant interest in the scientific community due to their unique properties of large surface area to volume ratio, superior tensile strength, and high porosity.[1−4] Various techniques, such as self-assembly,[5] phase separation,[6] drawing,[7] melt bowling,[8] electrospinning,[9] and template-directed synthesis,[10] allow for the creation of polymer nanofibrous membranes. Among them, electrospinning has emerged as an attractive nanotechnology for the production of nanofibers for biomimetic tissue scaffolding.[11] The nanoscale fineness of electrospun biomaterials provides a structural extracellular matrix (ECM) network

Received: May 31, 2015
Accepted: August 21, 2015
Published: August 21, 2015

DOI: 10.1021/acsami.5b04682
ACS Appl. Mater. Interfaces 2015, 7, 19672−19683

in which cells can grow during tissue repair and regeneration.[12] Therefore, electrospun nanofibrous membranes are widely used for tissue engineering, including in complex tissues such as liver, bone, heart, and muscle.[13] To achieve these applications, electrospun nanofibrous mats should possess biodegradability, biocompatibility, and sufficient mechanical strength.[14] A number of biomaterials, including natural and synthetic polymers and their composites, are being used to fabricate such scaffolds.[15,16] These include PCL, PVA, PVAc, PEO, PEG, PLGA, PLLA, cellulose, chitosan, alginate, and gelatin.[17] Among the various synthetic polymers, polycaprolactone (PCL) exhibits many advantages, such as good biodegradability, biocompatibility, excellent processability, and proper mechanical strength. Therefore, PCL has been extensively investigated over the last several decades, especially for use in the fields of biomedicine and tissue engineering.[18] Nevertheless, the low wettability and insufficient biocompatibility of PCL hinder its application in tissue engineering; these properties result in suboptimal adhesion, low spreading and growth of cells on the surface of the material, and a low hydraulic permeability through the scaffold.[19] Therefore, several modifications of PCL-based materials have been reported in order to improve their hydrophilic properties and to achieve a friendly interface for living cells. Recently, Ahmed et al. fabricated the coelectrospun PCL/cellulose composite mats using two nozzle electrospinning to improve the wicking properties of PCL nanofibers.[20] However, the individual fiber in the mat was either of the neat PCL or cellulose, not a hybrid of component polymers, and hence lacks the synergetic properties of component polymers. Blending PCL, a synthetic polymer, with a natural polymer on the nanoscale can easily improve its physicochemical properties for biomedical applications. Many efforts have been made to increase the hydrophilicity and biological activity of PCL nanofiber webs through incorporation of natural polymers, such as cellulose, gelatin,[11] chitosan,[21] keratin,[1] and alginate.[22] Although these studies have reported a favorable biological response to seeded cells such as enhanced cell attachment and in vitro cell proliferation, the material lacked the mechanical properties required for tissue engineering applications. Cellulose and its derivatives have been widely used to fabricate composite nanofibers with synthetic polymer.

Recent developments in cellulose research show that it is a promising biomaterial for tissue engineering, stem cell research, and regenerative medicine.[23] Bacterial-produced cellulose is primarily studied for bone regeneration.[24−27] However, it does not offer the ability to control the fibers on the nanoscale or microscale, which limits its applicability in tissue engineering.[28] Compared to cellulose, cellulose acetate (CA) is easy to process and has good spinability. In order to take advantage of the expanded processability window of CA, composite nanofibers can be produced using blending solutions of CA with synthetic polymers such as PCL; then, the CA content in a nanofiber can be easily hydrolyzed into cellulose through alkaline saponification.[29]

In this study, we improved the biological and physicochemical properties of PCL nanofiber for biomedical applications using cellulose chains. Here, a blend solution of PCL and CA with various compositions was electrospun to fabricate the nanofibrous membranes, and the resulting membranes were treated with NaOH solution to regenerate the cellulose chains in the individual nanofibers. The scaffolds were characterized in terms of morphology, physiochemical properties, biomimetic mineralization, and biocompatibility.

2. EXPERIMENTAL SECTION

2.1. Materials. In this study, poly(ε-caprolactone) (PCL, Mw = 70,000−90,000) and cellulose acetate (CA, Mw 30,000) were purchased from Sigma-Aldrich, USA; dimethylformamide (DMF), dichloromethane (DCM), acetone, *N*,*N*-dimethylacetamide (DMAc), and sodium hydroxide (NaOH) were purchased from Sam Chun, Korea. A 10 wt % PCL solution was prepared by dissolving PCL in a solvent system of DMF/DCM (4:1 w/w), and a 17 wt % CA solution was prepared in acetone/DMAc (2:1 w/w). Solutions were separately stirred for 12 h at room temperature and were then mixed at varying weight ratios so that the mass ratios of PCL and CA in the final solutions were 20:80, 40:60, 60:40, and 80:20. Mixed solutions were continuously stirred using a magnetic bar for 4 h prior to electrospinning.

2.2. Electrospinning process. A robot-controlled electrospinning setup was used in this study (Figure S1). The electrospinning solution (about 10 mL) was drawn into a 12 mL plastic syringe (NORM-JECT, Germany) connected to a metal capillary (di = 0.51 mm, 21 G) through a plastic tube. A digital syringe pump (New Era Pump System, Inc., USA) was used to control the flow rate (1 mL/h). Electrospinning was performed at ambient conditions (temperature ≈21 °C and humidity ≈28%) at a 17 kV applied voltage and a 15 cm tip-to-collector distance. During electrospinning, the nozzle moved sideways (i.e., horizontally) on its axis for a distance of 130 mm with a linear speed of 100 mm/min. Fibers were collected on the aluminum sheet attached to the surface of a ground iron drum. As-fabricated mats (PCL/CA) were vacuum-dried for 24 h at 25 °C and were dubbed M1, M2, M3, and M4 in order to represent the mats obtained by electrospinning of blend solutions with 20:80, 40:60, 60:40, and 80:20 mass ratios of PCL to CA, respectively.

2.3. Post-electrospinning treatment. The composite electrospun mats were carefully removed from the aluminum sheet and treated with a NaOH solution (0.05 M) in H_2O/ethanol (1:4 v/v) for 24 h in order to regenerate cellulose from cellulose acetate.[30] Regenerated cellulose-based membranes (PCL/CL) were thoroughly washed with distilled water until the wash solution becomes neutral and were named MR1, MR2, MR3, and MR4, corresponding to mats M1, M2, M3, and M4, respectively.

2.4. In vivo biomimetic mineralization. Simulated body fluid solution (SBF) was prepared using Hank's balanced salt (Aldrich, H2387-1) according to our previous report.[17] Briefly, a bottle of commercially available Hank's balanced salt along with $MgSO_4$ (0.097 g), $NaHCO_3$ (0.350 g), and $CaCl_2$ (0.185 g) were dissolved in 1 L distilled water. The pH of the solution was maintained at 7.4. The solution was filtered with 47 mm filter paper and stored at 5 °C for no longer than one month. PCL, PCL/CA, and PCL/CL mats were incubated in SBF solution for different time intervals at 37 °C. SBF solution was renewed every 24 h.

The deposition of calcium compounds on the SBF-treated mats was also evaluated using Alizarin Red S (ARS) assay according to a previous report.[31] Briefly, 10 days SBF treated samples (1 × 1 cm^2) were rinsed with DI water, fixed in 3.7% buffered formaldehyde for 30 min, and stained with 1 mL of ARS solution (40 mM, pH 4.1) in a 24-well plate for 20 min on an orbital shaker. Samples were then rinsed with DI water to remove the excess dye, transferred into another well plate, and treated with 50% acetic acid (1 mL) for 30 min. The dissolved dye was diluted with DI water in a 1:4 ratio, and pH was adjusted to 4.1. The absorbance of the solution was measured at 492 nm in a 96-well plate using a microplate reader (Sunrise Tecan, Austria).

2.5. In vitro biocompatibility. The viability of the cultured cell was monitored on the first, third, and seventh days of culture using a CCK (Dojindo's cell counting kit-8) assay. Samples (CA, PCL, PCL/CA, PCL/CL, and SBF-treated PCL/CL mats) of the same size were sterilized under UV light and thoroughly rinsed in phosphate buffer saline (pH 7.4). Later, samples were transferred to a 48-well plate and rinsed with medium prior to cell seeding. Cell (MC3T3-E1) suspension of 500 μL was seeded at a density of 1 × 10^4 cells/well and was incubated at 37 °C in a 5% CO_2 atmosphere. Culture medium

DOI: 10.1021/acsami.5b04682
ACS Appl. Mater. Interfaces 2015, 7, 19672−19683

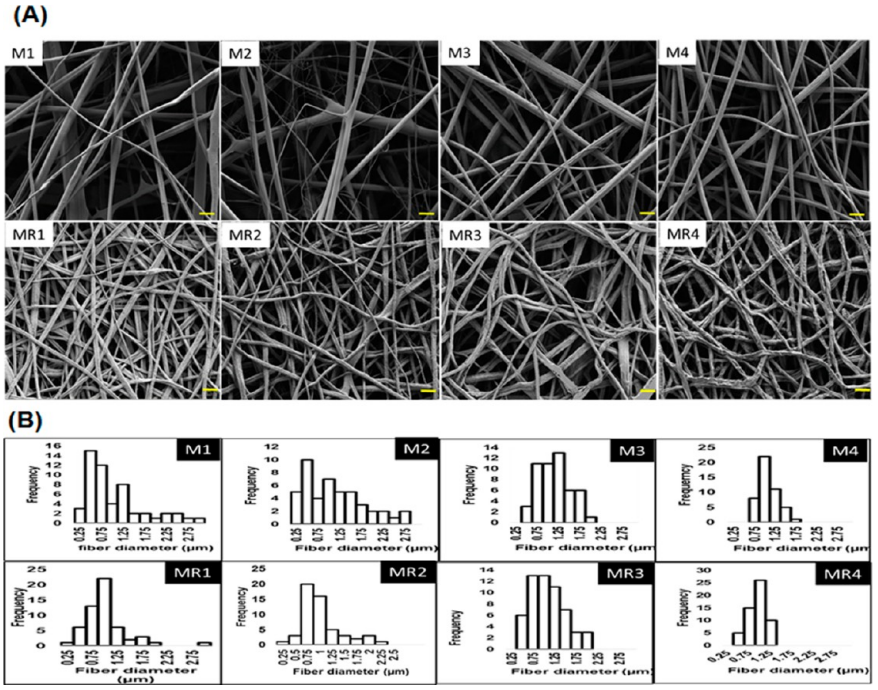

Figure 1. (A) FE-SEM images of composite mats before and after saponification. (B) Histogram showing fiber diameter distributions in different mats. (M1, M2, M3, and M4 represent the mats obtained by electrospinning of blend solutions with 20:80, 40:60, 60:40, and 80:20 mass ratios of PCL to CA, respectively, and MR1, MR2, MR3, and MR4 represent the saponified mats corresponding to M1, M2, M3, and M4 mats, respectively. Scale bar in FE-SEM images is 4 μm.)

Table 1. Viscosity and Conductivity of Different Solutions and Fiber Size Distribution in Corresponding Mats[a]

			Fiber diameter (μm)	
Solution/mat	Viscosity (cP)	Conductivity (ms/S)	Distribution	Mean ± SD
PCL/CA, 20:80 (M1)	1140 ± 12.78	0.550 ± 0.005	0.14−3.12	1.07 ± 1.04
PCL/CA, 40:60 (M2)	1020 ± 4.62	0.583 ± 0.002	0.17−3.41	1.08 ± 0.81
PCL/CA, 60:40 (M3)	704 ± 10.23	0.524 ± 0.003	0.34−1.58	1.07 ± 0.40
PCL/CA, 80:20 (M4)	512 ± 6.67	0.408 ± 0.026	0.71−1.34	0.95 ± 0.23
PCL/CL (MR1)			0.34−1.08	0.89 ± 0.52
PCL/CL (MR2)			0.16−1.10	0.84 ± 0.45
PCL/CL (MR3)			0.30−1.81	0.84 ± 0.33
PCL/CL (MR4)			0.27−1.16	0.81 ± 0.23

[a]PCL/CA solutions were prepared by blending PCL and CA solutions in different mass ratios. Conductivity and viscosity were measured three times for each solution, and average values are displayed in the table. M1, M2, M3, and M4 mats were fabricated by electrospinning the blend solutions, and corresponding MR1, MR2, MR3, and MR4 mats were achieved by alkaline saponification. The fiber diameter was measured using the ImageJ program, and the mean value with standard deviation is displayed.

was changed every 2 days. Following the manufacturer's instructions, 200 μL of cultured medium was transferred to a 96-well plate, and 20 μL of a CCK-8 solution was added to each well and incubated for 3 h. After 3 h of incubation, the absorbance was measured at a wavelength of 450 nm using a microplate reader (Sunrise Tecan, Austria). A standard curve was established by measuring the known number of cells prior to the experiment, and cell viability was determined from the standard curves. Among the groups, the cell viability of CA mat was set as control and the viability for other mats was expressed with its reference.

To examine cell attachment and spreading, samples were chemically fixed. The three- and seven-day cell cultured samples were rinsed with phosphate buffer saline (pH 7.4) and fixed with 2.5% glutaraldehyde for 1 h, followed by washing with 25%, 50%, 75%, and 100% ethanol for 20 min. They were dried overnight in a laminar flow hood. The cell morphology and attachment manner were determined via SEM.

In addition to SEM images, a confocal laser scanning microscope (Carl Zeiss, Japan) was employed to further confirm the cell biocompatibility and spreading behavior toward the scaffolds. Accordingly, cells were cultured on the scaffolds for a designated time (3 or 7 days) and stained with ActinGreen 488 and DAPI (4′,6-diamidino-2-phenylindole) (Life Technologies). Then, 4% paraformaldehyde was used to fix the cells, which were stained according to the manufacturer's protocol. Finally, the stained mats were examined using confocal laser scanning microscopy.

2.6. Scaffold characterization. Field emission scanning electron microscopy (FE-SEM, Carl Zeiss, Supra 40VP, Japan) was used to observe the surface morphology of different samples. ImageJ (NIH, USA) software was used to measure the fiber diameter. For each electrospun mat, more than 50 fibers were considered from five different images in order to calculate the average fiber diameter. The fabrication of PCL/CA composite fiber and saponification were determined by means of Fourier-transform infrared spectroscopy (FT-IR, ABB Bowen MB100 spectrometer, Canada) and X-ray diffraction patterns (XRD, Rigaku, Cu Kα λ = 1.540 A°, 30 kV, 40 mA). Thermal gravimetric analysis (TGA, Q50 TA Instruments) was used to investigate the thermal stability of different mats; the samples were heated from 30 to 800° at a rate of 10°/min. The surface wettability of

DOI: 10.1021/acsami.5b04682
ACS Appl. Mater. Interfaces 2015, 7, 19672−19683

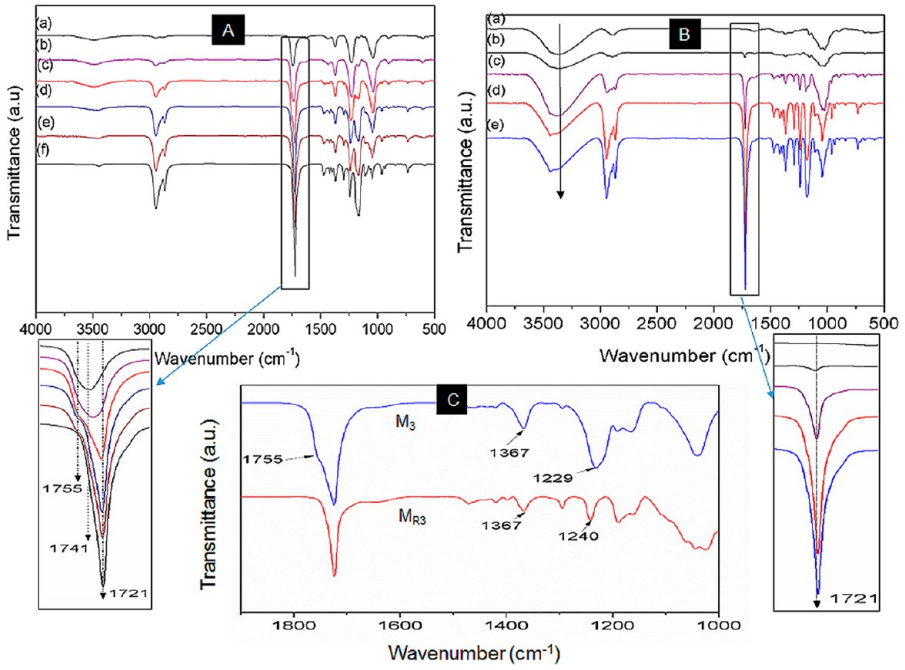

Figure 2. (A) FTIR spectra of (a) pristine CA mat, (b) M1, (c) M2, (d) M3, (e) M4, and (f) pristine PCL mat. (B) FTIR spectra after saponification of (a) regenerated cellulose, (b) MR1, (c) MR2, (d) MR3, and (e) MR4. (C) IR spectra showing the comparison between M3 and MR3.

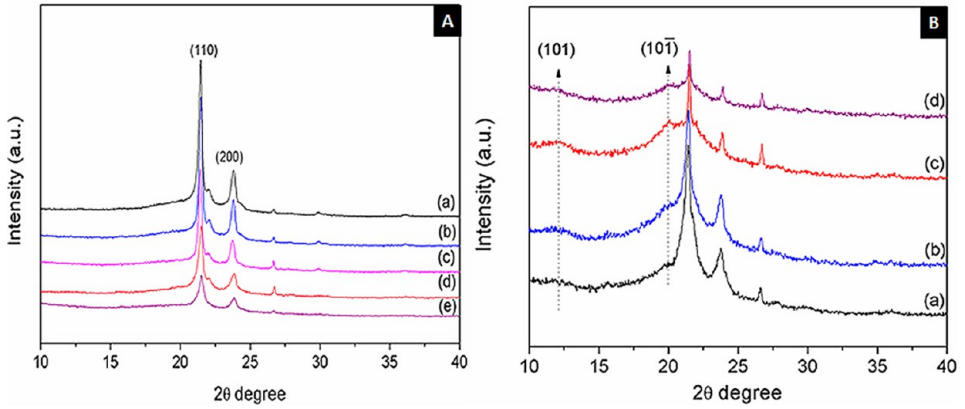

Figure 3. (A) XRD patterns of (a) pristine PCL nanofiber, (b) M1, (c) M2, (d) M3, and (e) M4. (B) XRD pattern after saponification of (a) MR1, (b) MR2, (c) MR3, and (d) MR4.

the electrospun membrane was determined measuring contact angle using DI water, glycerol, and diiodomethane by a contact angle meter (GBX, Digidrop, France). Liquid was automatically dropped (drop diameter 6 μm) onto the mat. The mechanical properties of the as-spun membranes were measured using an Instron mechanical tester (LLOYD instruments, LR5K plus, UK) using a dog-bone specimen based from ASTM D882-10.

3. RESULTS AND DISCUSSION

3.1. Physicochemical properties of the membrane. FE-SEM images of the electrospun mats compounded with different mass ratios of PCL and CA are presented in Figure 1A. All of the polymer compositions considered yielded bead-free nanofibers with no observable coagulation; however, the fiber morphology was noticeably changed. M1 and M2 mats (Figure 1A) showed tiny fiber-lets branched from primary nanofibers. The fiber diameter varied from the nanometer to micrometer range, and small splash defects were observed at the branches. Increasing the PCL composition of the matrix yielded more uniform, smooth, and compactly packed fibers without tiny fiber-lets (M3 and M4 mats, Figure 1A). The histogram of fiber diameter (Figure 1B) clearly shows that more uniform fibers were obtained at a lower composition of cellulose acetate in the electrospinning solution. The average fiber diameter gradually decreased from 1.07 to 0.81 μm with increasing PCL composition (Table 1, and Figure S2). The changes in fiber morphology and size distribution are attributed to changes in viscosity and conductivity of the blend solution. By increasing the PCL content in the blend solution, the viscosity gradually decreased from 1140 to 512 cP. Reduced viscosity results in smaller fiber diameter, due to the extent of elongation of the fibers being increased while being subjected to an electrical field.[32] Furthermore, reduced viscosity increased the spinability of the solution, resulting in fibers with uniform size distributions.[32]

Here, we intended to enrich the PCL nanofibers with cellulose chains. Therefore, PCL/CA composite mats were

DOI: 10.1021/acsami.5b04682
ACS Appl. Mater. Interfaces 2015, 7, 19672−19683

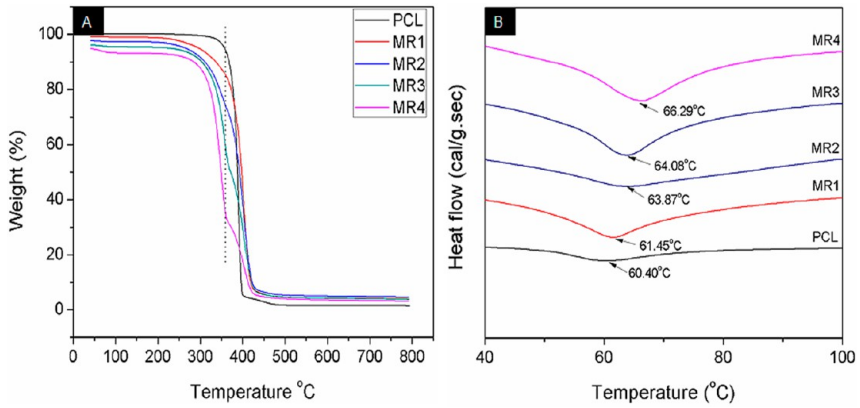

Figure 4. (A) TGA and (B) DSC curves of different composite mats.

treated with NaOH solution to regenerate cellulose via saponification.[30] The surface morphology of each membrane was dramatically changed after saponification; fibers were closely packed compared to those in corresponding PCL/CA mats (Figure 1A MR1-MR4). Such behavior was more pronounced in M1 and M2 membranes, where the smooth and cylindrical fibers became coarse and thin in corresponding MR1 and MR2 membranes. The fibers in the MR3 and MR4 membranes were more squeezed, stiff, and unevenly contracted throughout the membrane. The fibers were more uniform and the diameter was slightly decreased compared to a pristine PCL/CA membrane (Table 1). Regeneration of the crystalline cellulose chain from amorphous CA might have altered the packing of molecules in the fibers, resulting in a change in fiber morphology. These observations suggest that the regeneration of the cellulose in the fiber matrix has a substantial effect on the polymer interface and on fiber morphology.

FT-IR spectroscopy was employed to understand the molecular level interactions between the component polymers at different compositions. Figure 2A shows the FT-IR spectra of pristine and composite fibrous mats. The IR spectrum of the pristine PCL mat (Figure 2A, f) is characterized by the typical absorption bands at 2948 and 2868 cm^{-1} (stretching bands of CH_2 groups), 1721 cm^{-1} (stretching band of the ester group C═O), 1470 cm^{-1} (asymmetric deformation of CH_3), 1366 cm^{-1} (symmetric wagging of CH_3), 1294 and 1163 cm^{-1} (asymmetric and symmetric stretching of C−O−C), 1163 and 1108 cm^{-1} (asymmetric and symmetric stretching of C−O), 1240 cm^{-1} (CH_3 vibrations), 1046 cm^{-1} (C−O stretching and CH_2 rocking), and 1044 cm^{-1} (C−O stretching and CH bending).[33,34] Similarly, the IR results of pristine CA mat (Figure 3A, a) showed characteristic absorption bands at 1037 and 1228 cm^{-1} (C−O−C), 1368 cm^{-1} (C−CH_3), 1741 cm^{-1} (C═O from the acetyl groups), and 3482 cm^{-1} (O−H stretching of the hydroxyl groups).[30] The composite mats showed a gradual change in FT-IR spectra with varying compositions of PCL and CA in blend solutions (Figure S3). The peak intensities at 2948, 2868, 1721, 1470, 1294, 1163, 1108, and 1046 cm^{-1} were gradually increased with increasing PCL mass in electrospinning solution, i.e., peak intensity increased from M1 to M4 membranes. (The change in the IR band is clearly shown in Supporting Information Figure S3.) Absorption bands at 1037 and 1229 cm^{-1} (characteristics of C−O−C stretching of cellulose acetate) were steadily narrowed, the broad peak around 3482 cm^{-1} due to hydroxyl groups steadily decreased, and the peak corresponding to C═O at 1741 cm^{-1} was shifted to 1755 cm^{-1} with increasing PCL composition in the fibrous matrix. These results revealed that the CA and PCL solutions (described in the Experimental Section) have effective interaction at various compositions and can generate a composite nonwoven fibrous membrane. Figure 2B shows the FT-IR spectra of cellulose regenerated mats. The absorption bands related to PCL remained unchanged, while the absorption bands at 1229 and 1755 cm^{-1} related to the acetyl group and carbonyl group of cellulose acetate, respectively, disappeared in the spectrum of the saponified mats (Figures 2A−C and S3). Figure 2C is the comparison of the IR spectra of M3 and a corresponding saponified MR3 mat and clearly indicates the deacetylation of cellulose acetate. These results indicated the complete hydrolysis of cellulose acetate into cellulose. In addition, all the PCL/CL membranes (Figures 2B a−e) showed a broad and intense absorption band around 3300−3600 cm^{-1}, which is attributed to the hydroxyl group of regenerated cellulose.[35]

PCL is a semicrystalline polymer, and the presence of a foreign body in the fiber matrix can alter its crystallinity. Therefore, the effect of cellulose acetate on the crystallinity of the PCL fiber matrix was evaluated from the XRD patterns. Pristine PCL and PCL/CA membranes (Figure 3A) showed two strong diffraction peaks at 2θ = 21.4° (101) and 23.8° (200), characteristic of semicrystalline PCL nanofiber.[36] Compared to the pristine PCL mat, the peak intensity in the composite fiber matrix was gradually decreased with increasing CA mass (Figures 3A a−e), indicating a reduction in the degree of crystallinity of PCL.[37] The electrospinning process rapidly removes solvent, preventing preferred packing of polymer chains.[38] Furthermore, the presence of CA in the blend solution might have retarded the crystallization of PCL during the electrospinning process.[39]

Saponification of amorphous cellulose acetate into the crystalline cellulose chain changed the crystallinity of composite fibers, as is evident from the XRD pattern. All the regenerated mats showed new peaks around 2θ values of 12° (101), 20° ($10\bar{1}$), and 22° (002) (Figure 3B), a typical XRD pattern of cellulose II.[40] The peak intensities corresponding to cellulose II were gradually increased with increasing cellulose mass in the fiber matrix (Figure 3B), while that of PCL (at 2θ = 21.4° (101) and 23.8° (200)) was steadily decreased, revealing that the regeneration of the cellulose chain further affected the crystallinity of PCL in the composite fibers. This result also suggests that the crystallinity of PCL can be varied by varying the composition of cellulose acetate in the blend solution.

DOI: 10.1021/acsami.5b04682
ACS Appl. Mater. Interfaces 2015, 7, 19672−19683

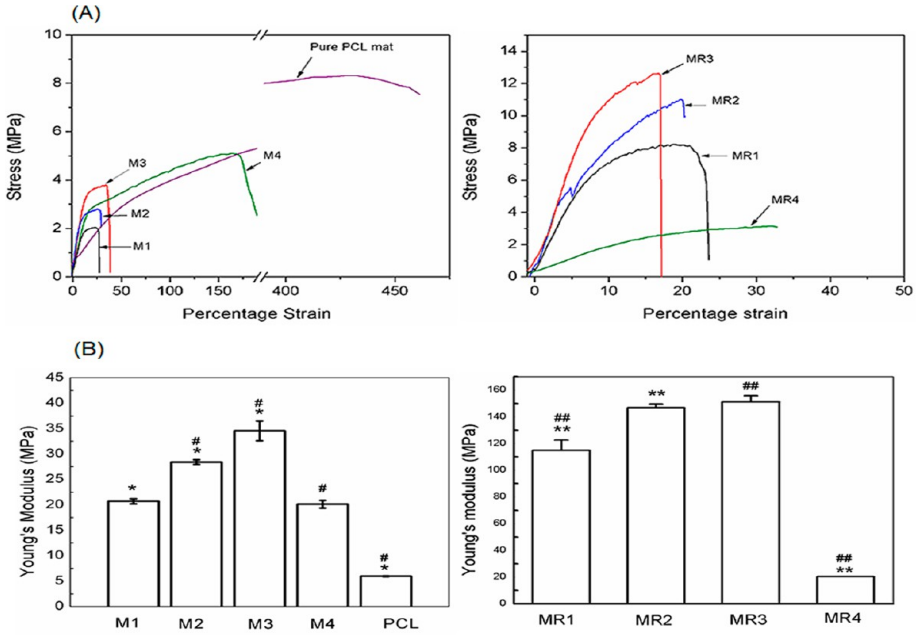

Figure 5. (A) Stress−strain curves for different mats. (B) Bar graph showing the Young's modulus for different mats; values were expressed as mean ± SEM (*, # $P < 0.05$ and **, ## $P < 0.01$; one-way ANOVA post hoc Tukey test).

Table 2. Tensile Properties of Various Samples[a]

Sample	Young's Modulus (MPa)	Tensile Strength (MPa)	Stress at Yield (MPa)	Percentage Strain at Maximum
M1	20.68 ± 0.09	1.91 ± 0.04	1.72 ± 0.11	23.83 ± 1.79
M2	28.53 ± 1.02	2.93 ± 0.17	2.82 ± 0.08	30.27 ± 2.36
M3	34.55 ± 3.28	3.5 ± 0.41	3.21 ± 0.62	32.32 ± 4.71
M4	20.16 ± 1.05	5.02 ± 0.13	2.85 ± 0.02	162.75 ± 4.59
MR1	114.93 ± 13.41	8.27 ± 0.081	7.7 ± 0.04	18.75 ± 0.63
MR2	146.71 ± 6.78	10.38 ± 1.38	7.2 ± 1.02	21.64 ± 2.02
MR3	151.39 ± 11.22	11.49 ± 1.68	10.41 ± 1.5	15.81 ± 1.20
MR4	20.23 ± 0.23	3.01 ± 0.18	2.73 ± 0.00	26.99 ± 6.65
PCL	5.92 ± 0.11	8.68 ± 0.299	4.2 ± 0.87	444.94 ± 14.45

[a]Each sample was evaluated three times. The mean values and corresponding standard deviation are displayed.

Control of the crystalline structure is expected to impact the in vivo stability and mechanical performance of the scaffold, providing a wider range of properties that can be controlled to impact scaffold performance.

The thermal behavior of pristine PCL and PCL/CL composite membranes was investigated using thermogravimetric analysis (TGA). The TGA curves (Figure 4A) exhibited a single-stage weight loss for PCL and a multistage weight loss for PCL/CL membranes. The first stage of weight loss (>200 °C) represents the loss of structural water molecules of the scaffold. Second-stage loss (starting at 305−326 °C) is attributed to the thermal degradation of cellulose, the third stage (starting around 385 °C) is due to decomposition, and the fourth stage (<400 °C) is attributed to the carbonization of polymeric material. The initial weight loss was proportional to the CL mass in the fiber matrix, which is attributed to the efficacy of CL to absorb moisture from the surroundings.[41] The percentage weight loss around 385 °C was increased with increasing amount of cellulose in the composite fibers (Figure 4A). Furthermore, the initial degradation temperature was also steadily reduced by increasing the CL mass in the composite fibers. This result revealed that most of the cellulose content of the fiber was degraded around 385 °C. DSC studies were also performed on the PCL and PCL/CL membranes (Figure 4B) in order to investigate the effect of cellulose on the structural properties of a PCL matrix. PCL nanofibers showed an endothermic peak around 60 °C, which is associated with its melting point.[42,43] An endothermic peak around 60 °C is also observed for PCL/CL composite nanofibers, with a slight right shift. This result revealed that a new material phase was formed at the different compositions without additional material phase.

Scaffolds must provide and retain sufficient mechanical support during cell proliferation and tissue regeneration without new-tissue deformation.[44] Therefore, scaffold mechanical properties were evaluated. The typical strain−stress curves of electrospun PCL/CA composite mats are presented in Figure 5A and S4. Table 2 summarizes the Young's Modulus, tensile strength, percentage strain, and stress at yield calculated from these curves. The tensile stress and Young's modulus were gradually increased with increasing PCL composition until the mass composition of PCL/CA is 60:40 in the fiber matrix and then decreased for 80:20. Each PCL/CA mat showed 4−7 times greater Young's modulus compared to a pristine PCL mat. Furthermore, the saponification of cellulose acetate significantly improved the mechanical properties of the fiber matrix. Interestingly, Young's modulus was gradually increased from MR1 to MR3 membranes, showing a 4−6 fold enhancement compared to those of PCL/CA mats and a

DOI: 10.1021/acsami.5b04682
ACS Appl. Mater. Interfaces 2015, 7, 19672−19683

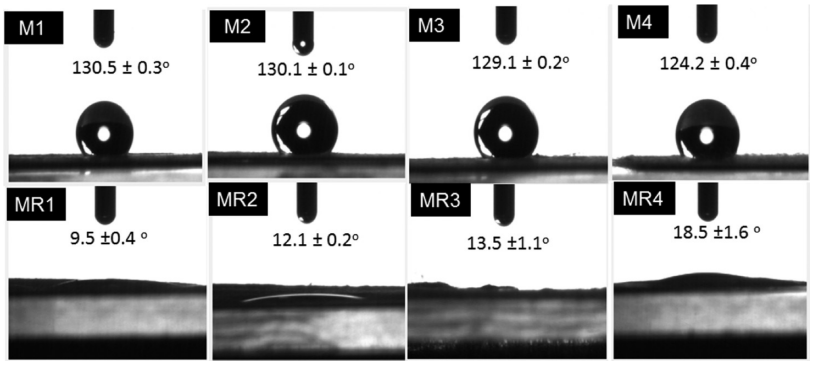

Figure 6. Water contact angle images of PCL/CA and corresponding saponified PCL/CL mats (mean ± SD, n = 3).

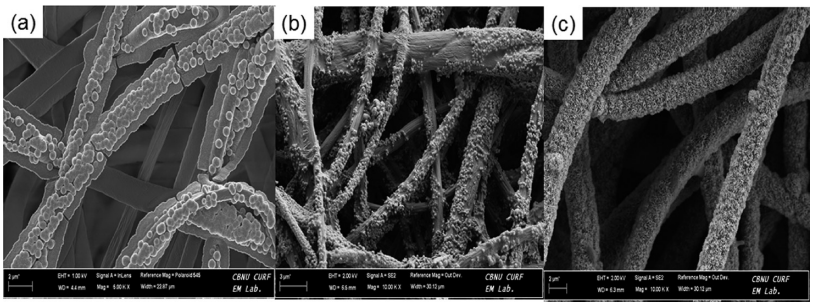

Figure 7. FE-SEM images of different samples exposed to SBF solution for 1 week: (a) neat PCL mat, (b) PCL/CA (M3) mat, (c) PCL/CL (MR3) mat.

20−30 fold enhancement compared to a pristine PCL mat (Figure 5B and Table 2). A similar trend was observed for tensile strength, and tensile stress. The enhancement in mechanical strength of the scaffold is attributed to regeneration of the cellulose chain in situ in the fiber matrix. Polar OH groups in regenerated cellulose are capable of forming inter-/intramolecular hydrogen bonding there by improving the mechanical properties of PCL/CL nanofibers compared to PCL/CA nanofibers. TEM images (Figure S5) and XRD patterns (Figure 3B) clearly showed the regeneration of cellulose nanocrystals in the nanofibers. Zoppe et al. reported that the cellulose nanocrystals in the fiber matrix greatly enhance the mechanical strength of nanofiber webs.[45] Furthermore, Young's modulus and tensile stress were gradually increased from MR1 to MR3 while they were sharply decreased for MR4 mat (Figure 5). The Young's modulus and tensile stress of MR4 mat were similar to that of M4 mat (Table 2), revealing that the mechanical properties were not improved after saponification for this mat. This result might be attributed to the following reasons: first, the cellulose regeneration in situ in the fiber might have affected the crystalline zone of PCL, but a very low content of regenerated cellulose in MR4 fibers was insufficient to compensate and boost the mechanical properties. Second, the Young's modulus and tensile stress were gradually increased with increasing PCL composition in the blend until the mass ratio of PCL/CA is 60:40 (M3) and then decreased for 80:20 (M4) (Figure 5B and Table 2), suggesting that the mass composition of PCL/CA above 60:40 has an inverse effect on those properties. This might be attributed to the low interfacial interaction of PCL and CA at higher mass composition of PCL in the blending solution, and a similar effect might have been reflected in MR4 mat. Miscibility and crystallization play crucial roles in the interfacial interaction and mechanical performance of polymer blends.[46] The existence of a miscibility window for blends of polymer with polymer/copolymer has been observed by several research groups.[47,48]

Scaffold wettability is known to be critical for biodegradation and biocompatibility for the aforementioned applications.[49,50] It influences the absorption of body fluid and transfer of nutrients and metabolities of the cells in the scaffolds.[51] Wettability also affects the cell suspension distribution in the scaffold and the structural morphology of regenerated tissue. Therefore, we evaluated the wettability of the scaffolds by measuring the contact angle using DI water, glycerol, and diiodomethane.

All the PCL/CA mats (Figure 6, M1-M4) showed a water contact angle larger than 124°, revealing typical hydrophobic surface characteristics. In contrast, the water contact angle was less than 20° for all the PCL/CL membranes (Figure 6, MR1-MR4). The pronounced increase in wettability is attributed to the hydroxyl groups of the cellulose chain in a composite mat.[52] To confirm these results, contact angles for another polar liquid, glycerol, were measured. The glycerol contact angles of 135.5, 136.5, 135.5, and 137.0 degree were observed for M1, M2, M3, and M4, respectively (Figure S6). This result suggests that all the PCL/CA mats have similar hydrophobic nature. The glycerol contact angles of 24.7, 28.2, 32.2, and 34.4 degree were observed for MR1, MR2, MR3, and MR4, respectively (Figure S6). The mass composition of CL gradually decreases from MR1 to MR4 mats; consequently, the number of polar hydroxyl groups decreased in the same trend. Decreasing the polar hydroxyl groups decreased the hydrophilicity from MR1 to MR4 mat. Furthermore, we measured the contact angle for the nonpolar liquid diiodomethane. A zero degree contact angle was observed for all PCL/CA mats (M1 to M4 mats) while 18.8, 15.5, 10.2, and 8.5 degree was observed for MR1, MR2, MR3, and MR4 mats, respectively (Figure S6). The gradual decrease in contact angle (increase in wettability) for a nonpolar liquid from MR1 to MR4 is attributed to the

DOI: 10.1021/acsami.5b04682
ACS Appl. Mater. Interfaces 2015, 7, 19672−19683

increased mass composition of PCL, a nonpolar polymer, in the nanofibers. Grafting PCL nanofibers with the cellulose chains not only improves the hydrophilicity, but also efficiently increases the tensile strength, surface polarity, and compatibility of the composite fiber by forming a network of strong hydrogen bonds.

3.2. Biomimetic coating of hydroxyapatite. In vitro incubation in the simulated body fluid (SBF) solution is a suitable technique to access the hydroxyapatite nucleation ability of a composite mat. The MR3 mat showed the superior mechanical properties compared to others. Therefore, the representative PCL/CA (M3), the corresponding PCL/CL (MR3), and the neat PCL mats were studied in order to evaluate their ability to nucleate hydroxyapatite (HA) in the SBF solution. It is interesting that the HA particles were only grown on the outer fibers of PCL, while the nanofibers beneath the surface layer remained smooth without HA crystals (Figure 7a). This is attributed to the strong hydrophobicity of the PCL mat, which had a water contact angle of 125.8° (Figure S7). The hydrophobic nature of the PCL nanofibers makes the capillary force ineffective. Therefore, the SBF solution could not penetrate to the inner fibers, limiting mineralization to the surface fibers.[53] On the other hand, the presence of the cellulose acetate in the PCL/CA mat (Figure 7b) retarded the mineralization process, as the cellulose acetate nanofibers have little efficiency for biomimetic mineralization (discussed in Supporting Information, Figure S8). Here, PCL/CL composite scaffolds (Figure 7c) showed deposition of HA crystal throughout the matrix. The superior performance of the PCL/CL mat is attributed to its improved wettability, which allowed the SBF solution to enter into the pores of the mat via capillary action, and the surface functional groups (hydroxyl group) assisted in the nucleation of HA particles. Deposition of calcium compounds on the 10 days SBF-treated mats was further studied using an Alizarin Res S (ARS) assay. Figure 8

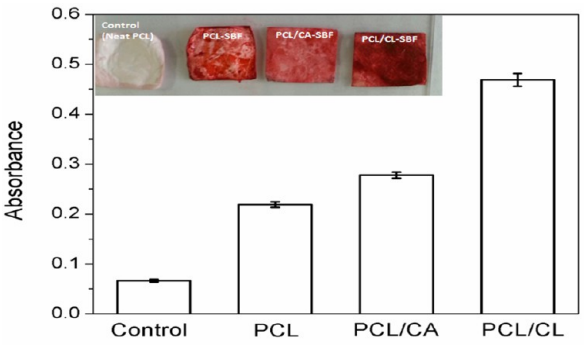

Figure 8. Absorbance shown by Alizarin Red S extracted from the stained calcium deposits in different mats treated with SBF solution for 10 days. The inset shows the digital images of different mats stained with alizarin Red S. (The neat PCL mat is used as control; absorbance was measured at 492 nm.)

shows the absorbance of Alizarin Red S extracted from the stained calcium deposits in different mats and corresponding digital images. Alizarin Red S extract from PCL/CL mat showed significantly higher absorbance value compared to the extract from PCL and PCL/CA mats (Figure 8), indicating the higher amount of calcium compounds in the PCL/CL fiber matrix.[31] Moreover, the digital image of an ARS stained PCL mat (Figure 8, inset) showed staining of entire surfaces with some difference in color intensities across the sample. A similar result was observed for PCL/CA mat while the PCL/CL mat showed the dark and homogeneous staining across the sample, revealing the deposition of more calcium compound throughout the fiber matrix, in agreement with FE-SEM images.

The chemical structure of a PCL/CL mat exposed to SBF solution for 1 week was investigated by comparing its XRD pattern with that of synthetic HA (Sigma-Aldrich). XRD peaks observed at 2θ values of 25.8°, 31.7°, 32.9°, 34.0°, 39.7°, 46.6°, 49.4°, and 53.2° correspond to synthetic HA (Figure 9B).[30] The XRD pattern of the mineralized mats was similar to that of the synthetic HA (Figure 9B); however, the peaks located between 25° and 35° were slightly broadened which might be due to the small size of crystallite or it might be due to the presence of amorphous Ca/P in the SBF-treated scaffold, similar to the previous reports.[30,54] Mahamid et al.[55] reported that a cluster of amorphous Ca/P minerals transforms into platelets of crystalline apatite within the collagen matrix. EDX analysis was performed to observe the elemental composition in a mineralized mat. The mole ratio of Ca/P was found to be 1.68 (Figure 9A), which is similar to the 1.67 of natural bone.[56] This result clearly indicates that the PCL/CL nanofiber can nucleate the calcium deficient HA, which resembles the natural bone.

3.3. In vitro biocompatibility. Investigation of cell viability is important to evaluate the biocompatibility of different biomaterials in vitro.[57] Therefore, osteoblast cells (MC3T3-E1 cell) were seeded onto the representative PCL, CA, PCL/CA (M3), PCL/CL (MR3), and PCL/CL-SBF (MR3 mat incubated in SBF solution for 1 week) mats for 1, 3, and 7 days. Cell viability was determined using the CCK assay. Each membrane exhibited a similar gradual growth pattern during the 24 h cell culture time (Figure 10). The PCL/CL mat showed slightly higher cell proliferation at 3 and 7 days, indicating that the regeneration of cellulose chain into the nanofibers accelerated the proliferation of the cells. This was likely due to the enhanced hydrophilicity and biocompatibility of biopolymer cellulose in the fiber matrix; alternatively, this might be due to the change in surface topography of the membrane. Moreover, the PCL/CL-SBF mat showed a significantly higher cell proliferation at 7 days compared to pristine PCL, PCL/CA, and PCL/CL mats (Figure 10), which is attributed to the HA particles on the surface of the nanofiber that provided improved biocompatibility to the membrane. The interaction between biomaterials and cells is considered the vital step toward tissue regeneration, so we evaluated this phenomenon via SEM and confocal images (Figures 11 and 12). The pristine PCL/CA mat (Figures 11a and b) showed aggregation of cellular mass into a small area, while the PCL/CL (Figures 11c and d) and PCL/CL-SBF mat (Figures 11e and f) showed the spreading of cellular mass throughout the surface of a mat with extended pseudopodia-like structure. Moreover, the PCL/CL-SBF mat showed enormous cells throughout the fiber matrix. These results suggest that the SBF-incubated mat had improved cell adhesion and proliferation compared to the PCL/CA and PCL/CL mats, revealing that the biomimetic mineralization of the nanofiber greatly improved the cell adhesion and proliferation. The improved biochemical interactions of cells with HA particles and the hydrophilicity of the composite scaffold might have provided good interactions compared to pristine PCL/CA and PCL/CL nanofibers. Cell morphologies were also confirmed using confocal laser scanning microscopy. The nuclei and cytoskeletons of cells on scaffolds were stained with DAPI and

DOI: 10.1021/acsami.5b04682
ACS Appl. Mater. Interfaces 2015, 7, 19672−19683

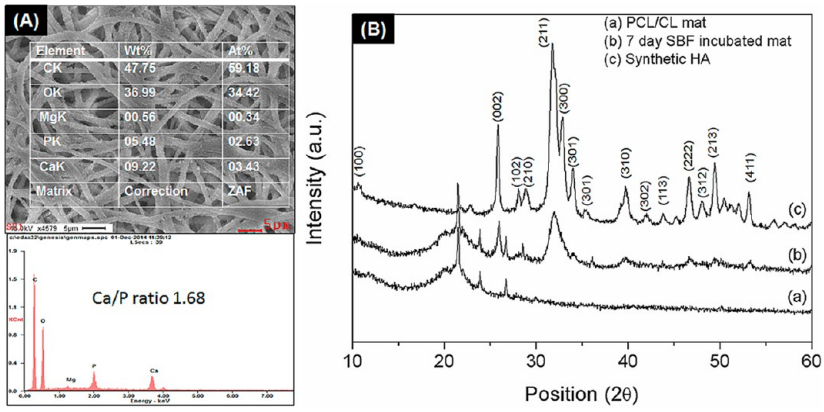

Figure 9. (A) EDX analysis of PCL/CL (MR3) mat exposed to simulated body fluid for 1 week. (B) XRD pattern of (a) PCL/CL mat, (b) PCL/CL mat exposed to simulated body fluid for 1 week, and (c) synthetic hydroxyapatite.

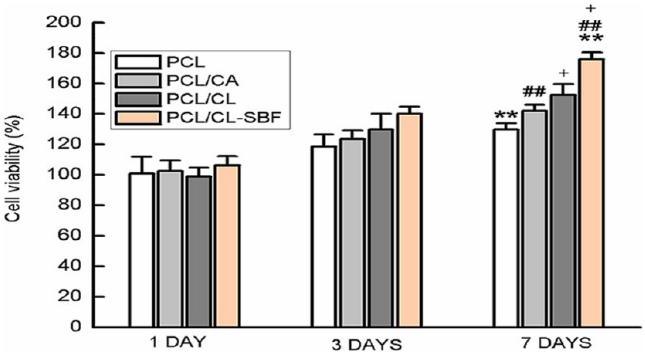

Figure 10. Graph showing the MC3T3-E1 cell viability indices for different mats on 1, 3, and 7 days. The viability of the control cell was set at 100%, and viability relative to control was expressed. All values were expressed as mean ± SEM. The data was individually analyzed with respect to days (**, ## $P < 0.01$; + $P < 0.05$; one way ANOVA post hoc Tukey test).

ActinGreen 488, respectively. As evidenced by the confocal images (Figure 12) after 3 and 7 days of incubation, MC3T3-E1 cells exhibited adhesion and spreading in descending order of SBF-incubated mat > PCL/CL mat > PCL/CA mat. Rounded nuclei with a cytoskeleton were distinctly observed in all samples. The SBF-incubated composite fibers showed profound cell growth throughout the mat, which might be due to the presence of extra bioactive HA coating. The cell–scaffold interaction observed by scanning electron microscopy was supported by confocal microscopy observations.

4. CONCLUSIONS

The present study represents an innovative strategy to fabricate the composite fibers of a barely spinnable polymer (cellulose) using its precursor (cellulose acetate) and subsequent post-electrospinning treatment. In this study, PCL/CL-based nanofibers were fabricated through the postmodification of electrospun PCL/CA nanofibers. CA and PCL solutions were blended to fabricate composite PCL/CA fibers, and subsequent hydrolysis by NaOH solution resulted in PCL/CL composite fibers. In situ regeneration of cellulose chain into the PCL fibers was confirmed by XRD, FT-IR, and TGA. As-fabricated nanofibers exhibited structural integrity, high wettability, and enhanced mechanical properties compared to the PCL and PCL/CA nanofibrous scaffolds. The ability for biomimetic mineralization throughout the matrix and excellent cellular compatibility revealed that as-synthesized PCL/CL composite scaffolds might be a potential candidate for future tissue regeneration applications.

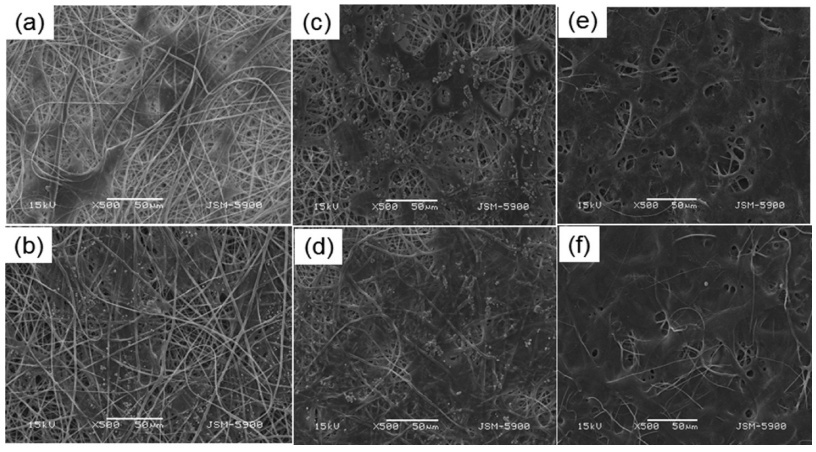

Figure 11. SEM images showing cell attachment on different scaffolds; (a, b) PCL/CA, (c, d) PCL/CL, and (e, f) SBF-incubated scaffolds at 3 days (a, c, e) and 7 days (b, d, f).

DOI: 10.1021/acsami.5b04682
ACS Appl. Mater. Interfaces 2015, 7, 19672–19683

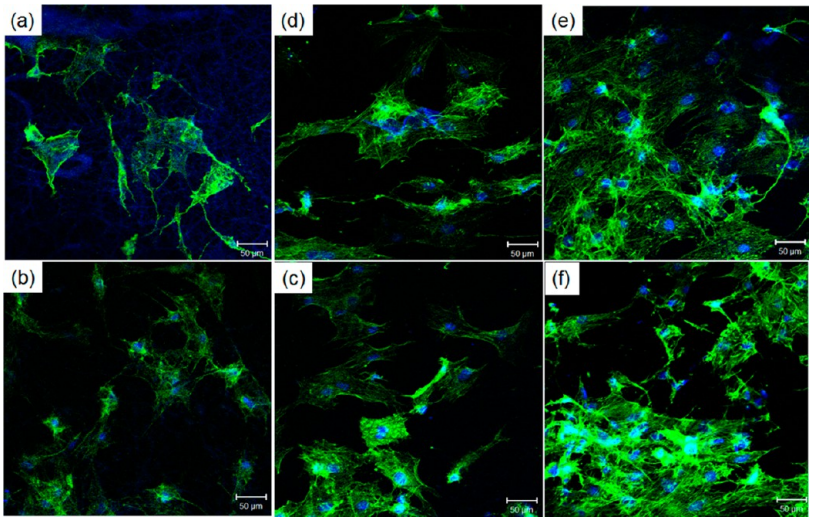

Figure 12. Confocal microscopy. Cells on scaffolds were stained with DAPI to display blue (nuclei) and ActinGreen 488 to display green (cytoskeleton). MC3T3-E1 activity on different scaffolds (a, b) PCL/CA, (c, d) PCL/CL, and (e, f) SBF-incubated PCL/CL mat. (a, c, e) represent 3 days, and (b, d, f) represent 7 days incubation.

■ ASSOCIATED CONTENT

Supporting Information

The Supporting Information is available free of charge on the ACS Publications website at DOI: 10.1021/acsami.5b04682.

FE-SEM images, FTIR spectra, TEM images, stress−strain curves for different mats, and contact angle using diiodomethane and glycerol (PDF)

■ AUTHOR INFORMATION

Corresponding Authors

*(Chan Hee Park) E-mail: biochan@jbnu.ac.kr.

*(Cheol Sang Kim) E-mail: chskim@jbnu.ac.kr. Tel.: +82-63-270-4284. fax: +82-63-270-2460.

Notes

The authors declare no competing financial interest.

■ ACKNOWLEDGMENTS

This research was supported by a grant from the Korean Ministry of Education, Science and Technology (MIST), through the National Research Foundation (NRF) (Project no. 2013 R1A2A2A04015484) and also partially by a grant from the Academy and Research Institute funded by the Korean Small and Medium Business Administration (project No. C0208053). We would also like to thank the Centre for University Research Facility (CURF), Chonbuk National University, for FE-SEM, TEM, and XRD analysis.

■ REFERENCES

(1) Edwards, A.; Jarvis, D.; Hopkins, T.; Pixley, S.; Bhattarai, N. Poly(E-Caprolactone)/Keratin-Based Composite Nanofibers for Biomedical Applications. *J. Biomed. Mater. Res., Part B* **2015**, *103*, 21−30.

(2) Peresin, M. S.; Habibi, Y.; Zoppe, J. O.; Pawlak, J. J.; Rojas, O. J. Nanofiber Composites of Polyvinyl Alcohol and Cellulose Nanocrystals: Manufacture and Characterization. *Biomacromolecules* **2010**, *11*, 674−681.

(3) Cui, W.; Li, X.; Zhou, S.; Weng, J. Investigation on Process Parameters of Electrospinning System through Orthogonal Experimental Design. *J. Appl. Polym. Sci.* **2007**, *103*, 3105−3112.

(4) GhavamiNejad, A.; Sasikala, A. R. K.; Unnithan, A. R.; Thomas, R. G.; Jeong, Y. Y.; Vatankhah-Varnoosfaderani, M.; Stadler, F. J.; Park, C. H.; Kim, C. S. Mussel-Inspired Electrospun Smart Magnetic Nanofibers for Hyperthermic Chemotherapy. *Adv. Funct. Mater.* **2015**, *25*, 2867−2875.

(5) Pal, J.; Sanwaria, S.; Srivastava, R.; Nandan, B.; Horechyy, A.; Stamm, M.; Chen, H.-L. Hairy Polymer Nanofibers Via Self-Assembly of Block Copolymers. *J. Mater. Chem.* **2012**, *22*, 25102−25107.

(6) Reneker, D. H.; Yarin, A. L. Electrospinning Jets and Polymer Nanofibers. *Polymer* **2008**, *49*, 2387−2425.

(7) Wang, P.; Wang, Y.; Tong, L. Functionalized Polymer Nanofibers: A Versatile Platform for Manipulating Light at the Nanoscale. *Light: Sci. Appl.* **2013**, *2*, e102.

(8) Dalton, P. D.; Grafahrend, D.; Klinkhammer, K.; Klee, D.; Möller, M. Electrospinning of Polymer Melts: Phenomenological Observations. *Polymer* **2007**, *48*, 6823−6833.

(9) Reneker, D. R.; Chun, I. Nanometre Diameter Fibres of Polymer, Produced by Electrospinning. *Nanotechnology* **1996**, *7*, 216.

(10) Tao, S. L.; Desai, T. A. Aligned Arrays of Biodegradable Poly(E-Caprolactone) Nanowires and Nanofibers by Template Synthesis. *Nano Lett.* **2007**, *7*, 1463−1468.

(11) Feng, B.; Tu, H.; Yuan, H.; Peng, H.; Zhang, Y. Acetic-Acid-Mediated Miscibility toward Electrospinning Homogeneous Composite Nanofibers of Gt/Pcl. *Biomacromolecules* **2012**, *13*, 3917−3925.

(12) Hughes, L. A.; Gaston, J.; McAlindon, K.; Woodhouse, K. A.; Thibeault, S. L. Electrospun Fiber Constructs for Vocal Fold Tissue Engineering: Effects of Alignment and Elastomeric Polypeptide Coating. *Acta Biomater.* **2015**, *13*, 111−120.

(13) Agarwal, S.; Wendorff, J. H.; Greiner, A. Use of Electrospinning Technique for Biomedical Applications. *Polymer* **2008**, *49*, 5603−5621.

(14) Jiang, T.; Carbone, E. J.; Lo, K. W. H.; Laurencin, C. T. Electrospinning of Polymer Nanofibers for Tissue Regeneration. *Prog. Polym. Sci.* **2015**, *46*, 1−24.

(15) Arcos, D.; Vallet-Regí, M. Sol−Gel Silica-Based Biomaterials and Bone Tissue Regeneration. *Acta Biomater.* **2010**, *6*, 2874−2888.

(16) Sabir, M.; Xu, X.; Li, L. A Review on Biodegradable Polymeric Materials for Bone Tissue Engineering Applications. *J. Mater. Sci.* **2009**, *44*, 5713−5724.

(17) Pant, H. R.; Risal, P.; Park, C. H.; Tijing, L. D.; Jeong, Y. J.; Kim, C. S. Core−Shell Structured Electrospun Biomimetic Composite Nanofibers of Calcium Lactate/Nylon-6 for Tissue Engineering. *Chem. Eng. J.* **2013**, *221*, 90−98.

(18) Pan, L.; Pei, X.; He, R.; Wan, Q.; Wang, J. Multiwall Carbon Nanotubes/Polycaprolactone Composites for Bone Tissue Engineering Application. *Colloids Surf., B* **2012**, *93*, 226−234.

(19) Zhang, Y. Z.; Venugopal, J.; Huang, Z. M.; Lim, C. T.; Ramakrishna, S. Characterization of the Surface Biocompatibility of

DOI: 10.1021/acsami.5b04682
ACS Appl. Mater. Interfaces 2015, 7, 19672−19683

the Electrospun Pcl-Collagen Nanofibers Using Fibroblasts. *Biomacromolecules* **2005**, *6*, 2583−2589.
(20) Ahmed, F.; Saleemi, S.; Khatri, Z.; Abro, M. I.; Kim, I.-S. Co-Electrospun Poly(ε-Caprolactone)/Cellulose Nanofibers-Fabrication and Characterization. *Carbohydr. Polym.* **2015**, *115*, 388−393.
(21) Bhattarai, N.; Li, Z.; Gunn, J.; Leung, M.; Cooper, A.; Edmondson, D.; Veiseh, O.; Chen, M.-H.; Zhang, Y.; Ellenbogen, R. G.; Zhang, M. Natural-Synthetic Polyblend Nanofibers for Biomedical Applications. *Adv. Mater.* **2009**, *21*, 2792−2797.
(22) Bhattarai, N.; Li, Z.; Edmondson, D.; Zhang, M. Alginate-Based Nanofibrous Scaffolds: Structural, Mechanical, and Biological Properties. *Adv. Mater.* **2006**, *18*, 1463−1467.
(23) Du, J.; Tan, E.; Kim, H. J.; Zhang, A.; Bhattacharya, R.; Yarema, K. J. Comparative Evaluation of Chitosan, Cellulose Acetate, and Polyethersulfone Nanofiber Scaffolds for Neural Differentiation. *Carbohydr. Polym.* **2014**, *99*, 483−490.
(24) Shi, Q.; Li, Y.; Sun, J.; Zhang, H.; Chen, L.; Chen, B.; Yang, H.; Wang, Z. The Osteogenesis of Bacterial Cellulose Scaffold Loaded with Bone Morphogenetic Protein-2. *Biomaterials* **2012**, *33*, 6644−6649.
(25) Xing, Q.; Zhao, F.; Chen, S.; McNamara, J.; DeCoster, M. A.; Lvov, Y. M. Porous Biocompatible Three-Dimensional Scaffolds of Cellulose Microfiber/Gelatin Composites for Cell Culture. *Acta Biomater.* **2010**, *6*, 2132−2139.
(26) Filion, T. M.; Kutikov, A.; Song, J. Chemically Modified Cellulose Fibrous Meshes for Use as Tissue Engineering Scaffolds. *Bioorg. Med. Chem. Lett.* **2011**, *21*, 5067−5070.
(27) Zaborowska, M.; Bodin, A.; Bäckdahl, H.; Popp, J.; Goldstein, A.; Gatenholm, P. Microporous Bacterial Cellulose as a Potential Scaffold for Bone Regeneration. *Acta Biomater.* **2010**, *6*, 2540−2547.
(28) Li, K.; Wang, J.; Liu, X.; Xiong, X.; Liu, H. Biomimetic Growth of Hydroxyapatite on Phosphorylated Electrospun Cellulose Nanofibers. *Carbohydr. Polym.* **2012**, *90*, 1573−1581.
(29) Zhou, C.; Shi, Q.; Guo, W.; Terrell, L.; Qureshi, A. T.; Hayes, D. J.; Wu, Q. Electrospun Bio-Nanocomposite Scaffolds for Bone Tissue Engineering by Cellulose Nanocrystals Reinforcing Maleic Anhydride Grafted Pla. *ACS Appl. Mater. Interfaces* **2013**, *5*, 3847−3854.
(30) Rodríguez, K.; Renneckar, S.; Gatenholm, P. Biomimetic Calcium Phosphate Crystal Mineralization on Electrospun Cellulose-Based Scaffolds. *ACS Appl. Mater. Interfaces* **2011**, *3*, 681−689.
(31) Madurantakam, P. A.; Rodriguez, I. A.; Cost, C. P.; Viswanathan, R.; Simpson, D. G.; Beckman, M. J.; Moon, P. C.; Bowlin, G. L. Multiple Factor Interactions in Biomimetic Mineralization of Electrospun Scaffolds. *Biomaterials* **2009**, *30*, 5456−5464.
(32) Deitzel, J. M.; Kleinmeyer, J.; Harris, D.; Tan, N. C. B. The Effect of Processing Variables on the Morphology of Electrospun Nanofibers and Textiles. *Polymer* **2001**, *42*, 261−272.
(33) Elzubair, A.; Elias, C. N.; Suarez, J. C.; Lopes, H. P.; Vieira, M. V. The Physical Characterization of a Thermoplastic Polymer for Endodontic Obturation. *J. Dent. (Oxford, U. K.)* **2006**, *34*, 784−9.
(34) Ding, Y.; Roether, J. A.; Boccaccini, A. R.; Schubert, D. W. Fabrication of Electrospun Poly (3-Hydroxybutyrate)/Poly (E-Caprolactone)/Silica Hybrid Fibermats with and without Calcium Addition. *Eur. Polym. J.* **2014**, *55*, 222−234.
(35) Montaño-Leyva, B.; Rodriguez-Felix, F.; Torres-Chávez, P.; Ramirez-Wong, B.; López-Cervantes, J.; Sanchez-Machado, D. Preparation and Characterization of Durum Wheat (Triticum Durum) Straw Cellulose Nanofibers by Electrospinning. *J. Agric. Food Chem.* **2011**, *59*, 870−875.
(36) Yeo, M. G.; Kim, G. H. Preparation and Characterization of 3d Composite Scaffolds Based on Rapid-Prototyped Pcl/B-Tcp Struts and Electrospun Pcl Coated with Collagen and Ha for Bone Regeneration. *Chem. Mater.* **2012**, *24*, 903−913.
(37) Martel-Estrada, S. A.; Martínez-Pérez, C. A.; Chacón-Nava, J. G.; García-Casillas, P. E.; Olivas-Armendariz, I. Synthesis and Thermo-Physical Properties of Chitosan/Poly(Dl-Lactide-Co-Glycolide) Composites Prepared by Thermally Induced Phase Separation. *Carbohydr. Polym.* **2010**, *81*, 775−783.
(38) Pant, H. R.; Baek, W.-i.; Nam, K.-T.; Jeong, I.-S.; Barakat, N. A. M.; Kim, H. Y. Effect of Lactic Acid on Polymer Crystallization Chain Conformation and Fiber Morphology in an Electrospun Nylon-6 Mat. *Polymer* **2011**, *52*, 4851−4856.
(39) Meng, Z. X.; Zheng, W.; Li, L.; Zheng, Y. F. Fabrication and Characterization of Three-Dimensional Nanofiber Membrance of Pcl−Mwcnts by Electrospinning. *Mater. Sci. Eng., C* **2010**, *30*, 1014−1021.
(40) Fink, H. P.; Hofmann, D.; Philipp, B. Some Aspects of Lateral Chain Order in Cellulosics from X-Ray Scattering. *Cellulose* **1995**, *2*, 51−70.
(41) Kargarzadeh, H.; Ahmad, I.; Abdullah, I.; Dufresne, A.; Zainudin, S.; Sheltami, R. Effects of Hydrolysis Conditions on the Morphology, Crystallinity, and Thermal Stability of Cellulose Nanocrystals Extracted from Kenaf Bast Fibers. *Cellulose* **2012**, *19*, 855−866.
(42) Kouhi, M.; Morshed, M.; Varshosaz, J.; Fathi, M. H. Poly (E-Caprolactone) Incorporated Bioactive Glass Nanoparticles and Simvastatin Nanocomposite Nanofibers: Preparation, Characterization and in Vitro Drug Release for Bone Regeneration Applications. *Chem. Eng. J.* **2013**, *228*, 1057−1065.
(43) Li, X.; Shi, J.; Dong, X.; Zhang, L.; Zeng, H. A Mesoporous Bioactive Glass/Polycaprolactone Composite Scaffold and Its Bioactivity Behavior. *J. Biomed. Mater. Res., Part A* **2008**, *84A*, 84−91.
(44) Joshi, M. K.; Pant, H. R.; Tiwari, A. P.; kim, H. J.; Park, C. H.; Kim, C. S. Multi-Layered Macroporous Three-Dimensional Nanofibrous Scaffold Via a Novel Gas Foaming Technique. *Chem. Eng. J.* **2015**, *275*, 79−88.
(45) Zoppe, J. O.; Peresin, M. S.; Habibi, Y.; Venditti, R. A.; Rojas, O. J. Reinforcing Poly(E-Caprolactone) Nanofibers with Cellulose Nanocrystals. *ACS Appl. Mater. Interfaces* **2009**, *1*, 1996−2004.
(46) Zhu, W.; Wang, X.; Chen, X.; Xu, K. Miscibility, Crystallization, and Mechanical Properties of Poly(3-Hydroxybutyrate-Co-4-Hydroxybutyrate)/ Poly(Butylene Succinate) Blends. *J. Appl. Polym. Sci.* **2009**, *114*, 3923−3931.
(47) Shashidhara, G. M.; Guruprasad, K. H.; Varadarajulu, A. Miscibility Studies on Blends of Cellulose Acetate and Nylon 6. *Eur. Polym. J.* **2002**, *38*, 611−614.
(48) Moore, J. A.; Kaur, S. Blends of Poly(Amide-Enaminonitrile) with Poly(Ethylene Oxide), Poly(4-Vinylpyridine), and Poly(N-Vinylpyrrolidone). *Macromolecules* **1998**, *31*, 328−335.
(49) Entcheva, E.; Bien, H.; Yin, L.; Chung, C.-Y.; Farrell, M.; Kostov, Y. Functional Cardiac Cell Constructs on Cellulose-Based Scaffolding. *Biomaterials* **2004**, *25*, 5753−5762.
(50) Liu, H.; Yin, Y.; Yao, K.; Ma, D.; Cui, L.; Cao, Y. Influence of the Concentrations of Hyaluronic Acid on the Properties and Biocompatibility of Cs−Gel−Ha Membranes. *Biomaterials* **2004**, *25*, 3523−3530.
(51) Yeo, M. G.; Kim, G. H. Preparation and Characterization of 3d Composite Scaffolds Based on Rapid-Prototyped Pcl/B-Tcp Struts and Electrospun Pcl Coated with Collagen and Ha for Bone Regeneration. *Chem. Mater.* **2012**, *24*, 903−913.
(52) Li, J.; Baker, B. A.; Mou, X.; Ren, N.; Qiu, J.; Boughton, R. I.; Liu, H. Biopolymer/Calcium Phosphate Scaffolds for Bone Tissue Engineering. *Adv. Healthcare Mater.* **2014**, *3*, 469−484.
(53) Wu, M.; Wang, Q.; Liu, X.; Liu, H. Biomimetic Synthesis and Characterization of Carbon Nanofiber/Hydroxyapatite Composite Scaffolds. *Carbon* **2013**, *51*, 335−345.
(54) Ye, M.; Mohanty, P.; Ghosh, G. Biomimetic Apatite-Coated Porous Pva Scaffolds Promote the Growth of Breast Cancer Cells. *Mater. Sci. Eng., C* **2014**, *44*, 310−316.
(55) Mahamid, J.; Aichmayer, B.; Shimoni, E.; Ziblat, R.; Li, C.; Siegel, S.; Paris, O.; Fratzl, P.; Weiner, S.; Addadi, L. Mapping Amorphous Calcium Phosphate Transformation into Crystalline Mineral from the Cell to the Bone in Zebrafish Fin Rays. *Proc. Natl. Acad. Sci. U. S. A.* **2010**, *107*, 6316−6321.
(56) Hutchens, S. A.; Benson, R. S.; Evans, B. R.; O'Neill, H. M.; Rawn, C. J. Biomimetic Synthesis of Calcium-Deficient Hydroxyapatite in a Natural Hydrogel. *Biomaterials* **2006**, *27*, 4661−4670.

DOI: 10.1021/acsami.5b04682
ACS Appl. Mater. Interfaces 2015, 7, 19672−19683

(57) Pant, H. R.; Kim, H. J.; Bhatt, L. R.; Joshi, M. K.; Kim, E. K.; Kim, J. I.; Abdal-hay, A.; Hui, K. S.; Kim, C. S. Chitin Butyrate Coated Electrospun Nylon-6 Fibers for Biomedical Applications. *Appl. Surf. Sci.* **2013**, *285* (Part B), 538−544.

DOI: 10.1021/acsami.5b04682
ACS Appl. Mater. Interfaces 2015, 7, 19672−19683